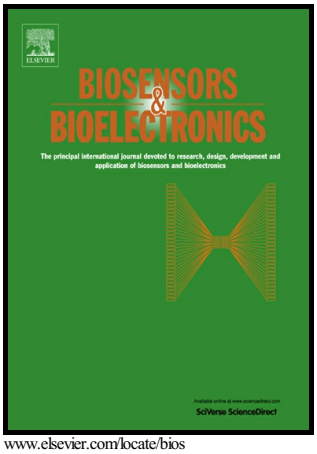

www.elsevier.com/locate/bios

Morphology-dependent Electrochemical Behavior of 18-facet Cu_7S_4 Nanocrystals Based Electrochemical Sensing Platform for Hydrogen Peroxide and Prostate Specific Antigen

Yuxue Dai, Xiaodong Zhu, Hao Liu, Yanna Lin, Weiyan Sun, Yuanling Sun, Chaofan Ding, Chuannan Luo, Qin Wei

PII: S0956-5663(18)30194-5
DOI: https://doi.org/10.1016/j.bios.2018.03.020
Reference: BIOS10346

To appear in: *Biosensors and Bioelectronic*

Received date: 27 December 2017
Revised date: 2 March 2018
Accepted date: 12 March 2018

Cite this article as: Yuxue Dai, Xiaodong Zhu, Hao Liu, Yanna Lin, Weiyan Sun, Yuanling Sun, Chaofan Ding, Chuannan Luo and Qin Wei, Morphology-dependent Electrochemical Behavior of 18-facet Cu_7S_4 Nanocrystals Based Electrochemical Sensing Platform for Hydrogen Peroxide and Prostate Specific Antigen, *Biosensors and Bioelectronic,* https://doi.org/10.1016/j.bios.2018.03.020

Morphology-dependent Electrochemical Behavior of 18-facet Cu_7S_4 Nanocrystals Based Electrochemical Sensing Platform for Hydrogen Peroxide and Prostate Specific Antigen

Yuxue Dai, Xiaodong Zhu, Hao Liu, Yanna Lin, Weiyan Sun, Yuanling Sun, Chaofan Ding, Chuannan Luo*, Qin Wei

Key Laboratory of Interfacial Reaction & Sensing Analysis in Universities of Shandong, School of Chemistry and Chemical Engineering, University of Jinan, Jinan 250022, PR China

Corresponding author. Chuannan Luo

Correspondence: chm_yfl518@163.com

Tel: 86-531 89736065

Abstract

18-facet polyhedron Cu_7S_4 nanocrystal and CuS sphere were prepared from Cu_2O precursor, and CuS flower was synthesized through a simple solvothermal approach. Their electrochemical performances were investigated towards H_2O_2 and it was interesting to discover that Cu_7S_4 nanocrystal had the best electrochemical catalysis compared with CuS sphere and CuS flower. It can deduce that the special structure of Cu_7S_4 nanocrystal endowed it more exposed active points, higher surface area and higher Cu/S ratio. Therefore, Cu_7S_4 nanocrystal was firstly employed to prepare a nonenzymatic biosensor for H_2O_2. Satisfactory results were obtained. In addition, a label-free sensing platform for prostate specific antigen (PSA) was

constructed based on electrochemical catalysis towards H_2O_2 of Cu_7S_4 nanocrystal. The label-free immunosenosr offered accurate PSA in the range of 0.001~15 ng/mL with the detection limit of 0.001 ng/mL. Besides, the immunosensor possessed good sensitivity, selectivity and stability and could detect PSA in real sample. More importantly, this work demonstrated that Cu_7S_4 nanocrystal hold great promising application in electrochemical sensors.

Keywords: 18-facet polyhedron Cu_7S_4 nanocrystals, CuS sphere, CuS flower, H_2O_2, prostate specific antigen

1. Introduction

Recently, transition metal dichalcogenides (TMDs) have been the hotspot for their original structures, outstanding electronic and optical properties as well as their wide applications (Su et al., 2017; Zhao et al., 2017; Rong et al., 2015; Peng et al., 2017). Copper sulphide (Cu_xS), one of TMDs, has been widely used in solar cells (Mousavi-Kamazani et al., 2016), lithium-ion batteries (Han et al., 2011), optical catalysis (Adhikari et al., 2017), thermoelectric and photoelectric transformers (Chen et al., 2017), superconductors (Raveau et al., 2011), and sensors (Yu et al., 2009; Fu, 2013; Yang et al., 2016; Fan et al., 2016) due to unique optical, electrical and thermal properties.

Various different morphologies of Cu_xS have been synthesized, including sphere (Heydari et al., 2017), hexagonal (Liu et al., 2013), hollow cube (Cai et al., 2015),

wire (Chen et al., 2008) and polyhedron (He et al., 2012) and so on and some of them have already been used for eletrochemical applications. Kim et al prepared CuS dendrite for glucose through electro-deposition and vapor-phase sulfurization (Kim et al., 2017). Qian et al synthesized CuS nanotubes for glucose through a simple self-sacrificial template method (Qian et al., 2013). Dutta et al prepared CuS nanoparticle for H_2O_2 and human blood glucose through a solvothermal approach (Dutta et al., 2014; Dutta et al., 2013). Lin et al synthesized sphere-like CuS microcrystals for glucose through solvothermal (Lin et al., 2013). However, CuS usually combines with other nanomaterials such as graphene (Shi et al., 2015), carbon nanotube (Zhang et al., 2016) to expand its application in the fabrication of electrochemical sensors to promote the limited electrochemical property.

Cu_7S_4, as a member of the nonstoichiometric copper sulfides, has also sparked wide interest, too (Chen et al., 2009; Jiang et al., 2014; Yu et al., 2016). Cu_7S_4 has been used in electrocatalysis, electrochemical detection, photothermal. Chen et al synthesized skeletal Cu_7S_4 nanocage for efficient counter electrode (Chen et al., 2015). Li et al prepared cobalt doped Cu_7S_4 nanodisk for oxygen evolution reaction (Li et al., 2017). Cui et al synthesized MoS_2 decorated Cu_7S_4-Au nanocatalyst for mercury (Cui et al., 2017). However, there is little report about Cu_7S_4 nanocrystal applied in electrochemical sensors.

Recenty, label-free immunosensors have attracted more interest due to its simple preparation and operation process compared with sandwich immunosensor (Jia et al., 2014; Ma et al., 2016; Wang et al., 2015). Wang et al prepared a label-free

immunosensor based on ultralong copper sulfide nanowires with a detection limit of 0.1 pg/mL. Jia et al synthesized graphene nanocomposites which was used to simultaneously determine multiple tumor markers through electrochemical technology.

Herein, Cu_7S_4 nanocrystal was synthesized through simple solvothermal method. In order to investigate the effect of its morphology on electrochemical behavior, CuS sphere and CuS flower were also prepared. Their electrochemical behavior towards H_2O_2 was investigated and it was interesting to discover that Cu_7S_4 nanocrystal had the best electrochemical catalysis. According to the result, it can infer that the morphology and Cu/S ratio played important role in their electrochemical properties. Compared with CuS sphere and CuS flower, the special structure of Cu_7S_4 nanocrystal endowed it more exposed active points, higher surface area and higher Cu/S ratio. Therefore, the biosensor was used to detect H_2O_2 based on Cu_7S_4 nanocrystal. and satisfactory results were obtained. In addition, Cu_7S_4 nanocrystal was also used to construct a label-free electrochemical immunosensor for PSA on the basis of its electrochemical catalysis towards H_2O_2. In this work, PSA was chosen as the model. Generally, when the level of serum PSA is less than 4.0 ng/mL, it is normal; when the concentration of PSA is greater than 10 ng/mL, the risk of pre-adenocarcinoma increases (Oberpenning et al., 2003). The immunosensor exhibited good sensitivity, selectivity and stability. Importantly, the proposed immunosensor was used to detect PSA in real sample and the result was acceptable.

2. Experimental section

2.1. Reagents and Solutions and Equipment.

The detail was shown in Supporting Information

2.2. Preparation of Cu_7S_4 nanocrystal, CuS spheres and flower-like CuS.

The detail was shown in Supporting Information.

2.2. Fabrication of H_2O_2 sensor and label-free immunosensor

Figure 1 showed the fabrication procedure of H_2O_2 biosensor and the label-free immunosensor. GCE was polished repeatedly using alumina powder and then thoroughly cleaned before use. To prepare H_2O_2 biosensor, 7 μL of 2 mg/mL Cu_7S_4 nanocrystal 0.1 % chitosan solution (in 0.1 M acetic acid) was coated on GCE. Then Cu_7S_4 nanocrystal/GCE was obtained to detect H_2O_2. CuS sphere and CuS flower modified GCE were also prepared in the same way for comparision. For electrochemical immunosensor, after Cu_7S_4 nanocrystal/GCE was dried and washed with PBS solution, 7 μL of glutaraldehyde solution was dropped. After 1 h, 7 μL anti-PSA (10 μg/mL) solution was dropped onto the electrode. The modified electrode was washed with PBS solution after 1 h and incubated in 1 wt.% BSA solution for 1 h to eliminate nonspecific binding between PSA and the electrode surface. Finally, 7 μL of different concentrations of PSA solution was coated onto the electrode surface and incubated for another 1 h, and was rinsed to remove unbound PSA on the outer surface.

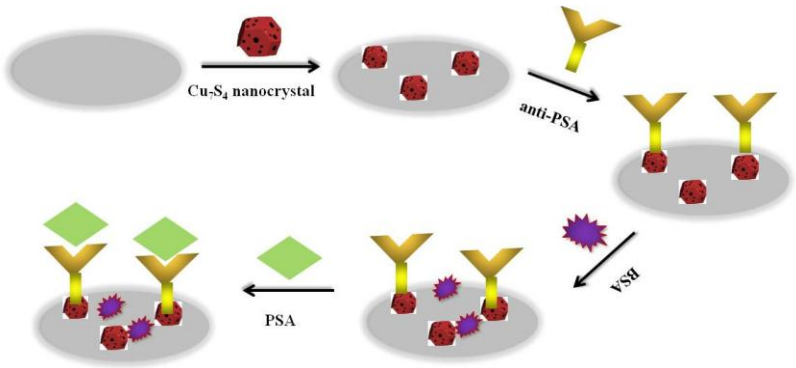

Figure 1 Fabrication steps of the immunosensor

3.Result and discussion

3.1. Characterization of Cu_2O cube, Cu_7S_4 nanocrystal, CuS sphere and CuS flower

It was inspired by the literature that the facet of Cu_2O crystals had great effect on its electrical conductivity (Tan et al., 2015). In this paper, Cu_7S_4 nanocrystal, CuS sphere and CuS flower were synthesized in order to investigate the effect of their morphology on the electrochemical catalysis. SEM and TEM were used to characterize morphology of Cu_2O cube, Cu_7S_4 nanocrystal, CuS sphere and CuS flower. As shown in Figure 2A and Figure S1A, Cu_2O with cubic crystal was observed with about 500 nm in length. Cu_7S_4 nanocrystal, CuS sphere were synthesized through Cu_2O precursor. Cu_7S_4 nanocrystal with high symmetric 18-face polyhedron nanocrystals was shown in Figure 2B and Figure S1B around 320 nm in particle size in line with the previous report (Cao et al., 2005). For CuS sphere, it was clearly observed that rough surface of CuS sphere was about 200~300 nm in diameter indicating that CuS sphere was successfully prepared (Figure 2C and Figure S1C)

(Heydari et al., 2017). Figure 2D showed that CuS flower adopted flower-like morphology composed of CuS sheet in accordance with the reported literature (Hu et al., 2017).

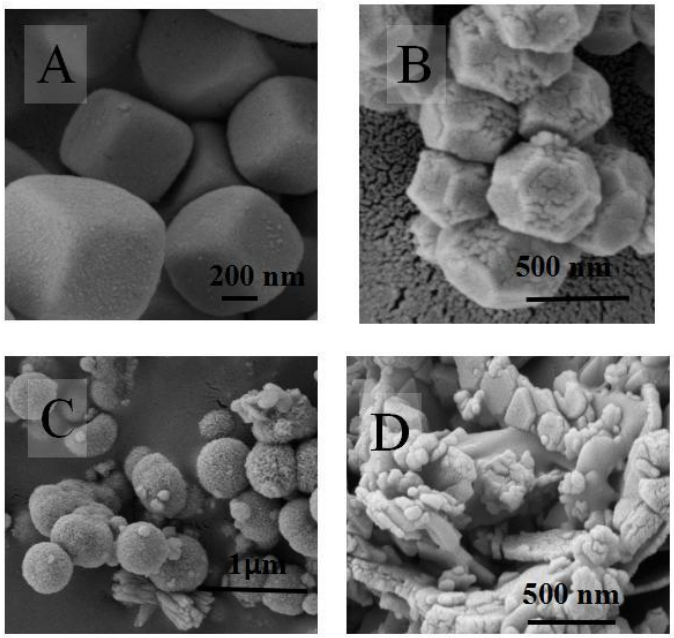

Figure 2 SEM of Cu_2O cube (A), Cu_7S_4 nanocrystal (B), CuS sphere (C) and CuS flower (D).

3.2. Electrochemical behavior of Cu_7S_4 nanocrystal, CuS sphere and CuS flower

To understand the electrochemical behavior of Cu_7S_4 nanocrystal, CuS sphere and CuS flower, cyclic voltammetry (CV) was recorded in pH=7.4 PBS solution with 2 mmol/L $K_3[Fe(CN)_6]$ and 0.1 mol/L KCl solution. From Figure 3A, bare GCE showed a couple of redox peak. After GCE was coated with Cu_7S_4 nanocrystal (curve b), the peak current declined somewhat compared with GCE. When CuS sphere and CuS flower were dropped on GCE respectively, the peak current decreased sharply compared with GCE. It could be ascribed to the unique properties of Cu_7S_4 nanocrystal, CuS sphere and CuS flower which were semiconductor. They would hinder electron transfer. Besides, the morphology also played important role in that

the peak current of Cu_7S_4 nanocrystal was larger than that of CuS sphere and CuS flower. The reason was that Cu_7S_4 nanocrystal had the largest surface area among them in accordance with the above results.

To verify the infer, chronocoulometry combined with Anson equation was used to calculate the area of the modified electrode (A) in 2 mM $K_3[Fe(CN)_6]$ solution. The asymptotic line of curve of the measured charge (Q) versus square root of time ($t^{1/2}$) satisfied the Anson equation:

$$Q = 2nFAc_0D^{0.5}t^{0.5}\pi^{-0.5} + Q_{dl} + Q_{ads} \quad (1)$$

Where Q was the total charge, n was the number of the electrons transferred per molecule ($[Fe(CN)_6]^{4-} - e^- \rightarrow [Fe(CN)_6]^{3-}$, n=1 in the reaction), F was the Faraday constant, c_0 was the concentration of analyte, D was the diffusion coefficient (7.6×10^{-6} cm^2s^{-1} for $K_3[Fe(CN)_6]$), t was the time, A was the area of the electrode, Q_{ads} was adsorbed charging and Q_{dl} was the double layer charging. Graphing Q at $t^{1/2}$ yielded a slope of $2nFAc_0D^{0.5}t^{0.5}\pi^{-0.5}$. As a result, the electrochemical active area of the electrode was calculated. As shown in Figure 3B, Q-$t^{1/2}$ of GCE showed the highest slop, then the slops of Cu_7S_4 nanocrystal, CuS sphere and CuS flower declined in turn indicating that GCE had the largest active area, then Cu_7S_4 nanocrystal, CuS sphere and CuS flower. The slope for GCE, Cu_7S_4 nanocrystal, CuS sphere and CuS flower was 6.5×10^{-3}, 5.5×10^{-3}, 4.2×10^{-3} and 1.0×10^{-7}, respectively. Furthermore, it can be calculated that the active area for GCE, Cu_7S_4 nanocrystal, CuS sphere and CuS flower was 0.146 cm^2, 0.123cm^2, 0.095 cm^2 and 4.46×10^{-5} cm^2, respectively. It could be observed that Cu_7S_4 nanocrystal had the closest active area of GCE due to its

special structure. The result proved that the morphology and surface area had remarkable effect on the electrochemical performance of Cu_7S_4 nanocrystal.

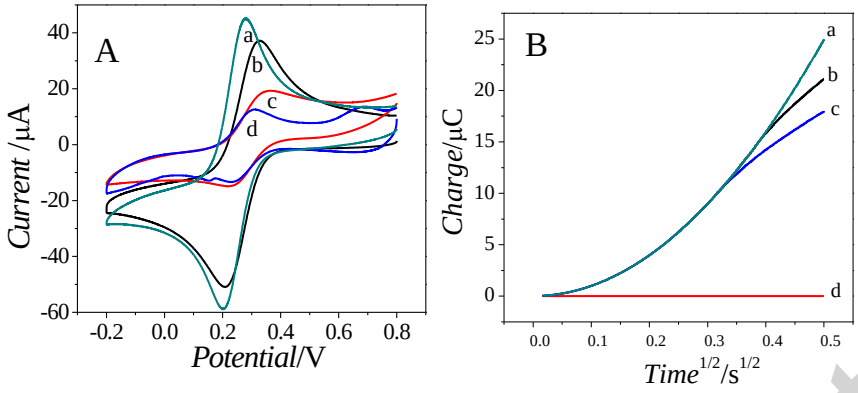

Figure 3 CVs (A) and Q-$t^{1/2}$ (B) of GCE (a), Cu_7S_4 nanocrystal (b), CuS sphere (c) and CuS flower (d) in pH=7.4 PBS solution with 2 mmol/L $K_3[Fe(CN)_6]$ and 0.1 mol/L KCl solution.

The electrochemical behavior of Cu_7S_4 nanocrystal, CuS sphere and CuS flower towards H_2O_2 was investigated. In addition, the current change at -0.6 V in the absence and presence of of 10 mM H_2O_2 (ΔI) was used to evaluate the electrocatalysis ability of the modified electrode. From Figure 4A, it was easily observed that GCE had little electrocatalysis towards H_2O_2. After GCE was modified with Cu_7S_4 nanocrystal, CuS sphere and CuS flower, ΔI of Cu_7S_4 nanocrystal was 2.7 times and 22 times larger than CuS sphere and CuS flower respectively as Figure 4B, Figure 4C and Figure 4D showed, indicating that Cu_7S_4 nanocrystal had the best electrochemical catalytic ability towards H_2O_2. Besides, it was obviously observed that there was a broad peak at +0.3 V in Figure 4B, Figure 4C and Figure 4D ascribed to Cu^{2+}/Cu^{3+} (Kim et al., 2017; Qian et al., 2013). And the peak at -0.65 V could be due to the transition of Cu^{2+} to Cu^{+}. Upon additon of 10 mM H_2O_2, peak at +0.3 V increased in Figure 4B and Figure 4C while it showed little change in Figure 4D. There may be the

following reasons. First, Cu^{+} existed in CuS and CuS reacted with H_2O_2 forming Cu^{2+} leading to the increase of the peak current at +0.3 V. Second, Cu_7S_4 nanocrystal had more active sites that could also promote the electrochemical catalysis compared with CuS sphere and CuS flower in that polyhedron nanocrystals of Cu_7S_4 endowed it larger surface area and more exposed active sites. Third, Cu/S ratio had certain effect too and Cu/S ratio of Cu_7S_4 nanocrystal was 1.75 (Cao et al., 2005). For the foregoing reasons, Cu_7S_4 nanocrystal had the best elctrocatalytic ability towards H_2O_2.

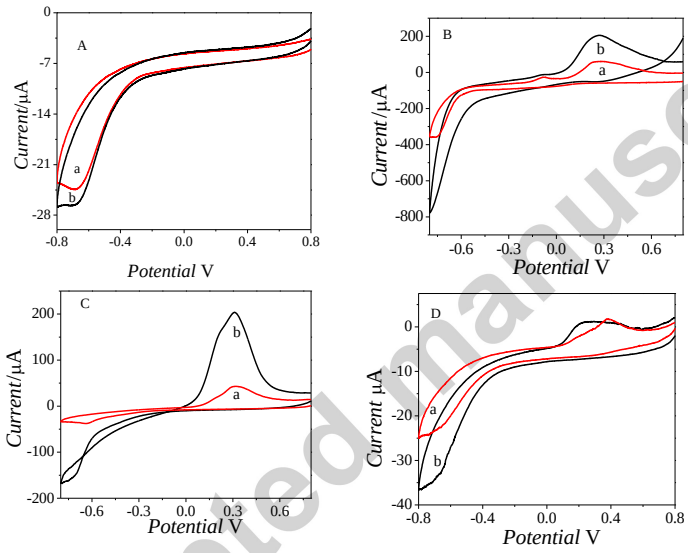

Figure 4 (A) CVs of bare GCE (A), Cu_7S_4 nanocrystal (B), CuS sphere (C) and CuS flower (D) in pH=7.4 PBS solution in the absence (a) and presence of of 10 mM H_2O_2 (b).

To further prove the the catalytic performance of Cu_7S_4 nanocrystal, CuS sphere and CuS flower, the amperometric i-t curve was recorded at -0.6 V in PBS solution (pH=7.4) with successful addition of 10 mM H_2O_2. From Figure S2, bare GCE showed little catalytic effect towards H_2O_2 (curve a) and the current response of CuS flower (curve b) was too small to affect the catalytic response. When CuS sphere was

coated on GCE, a significant increase was observed (curve c). After Cu_7S_4 nanocrystal was coated on GCE (curve d), a larger current response was obtained in line with the previous results.

3.3. Optimization of experimental conditions

3.3.1 pH

Since it was discovered that Cu_7S_4 nanocrystal had good electrocatalytic ability towards H_2O_2, a biosensor was constructed. pH had important effect on the electrochemical performance of biosensor. It could be observed that the current change reached maximum at 7.4 (Figure S3A). So 7.4 was chosen as the pH value of solution for the electrochemical determination of H_2O_2.

3.3.2 Concentration of Cu_7S_4 nanocrystal

The effect of concentration of Cu_7S_4 nanocrystal towards H_2O_2 was investigated. As shown in Figure S3B, current change increased with increasing concentration of Cu_7S_4 nanocrystal firstly and reached the maximum at 2 mg/mL. While concentration of Cu_7S_4 nanocrystal further increased, current change decreased. That was when the concentration was too high, and the film of the modified electrode would become too thick resulting in hindering electron transfer. As a result, 2 mg/mL of Cu_7S_4 nanocrystal was chosen for the following experiments.

3.4. Electrochemical characterization of the biosensor

Under optimal experimental condition, the biosensor towards different concentrations of H_2O_2 was recorded as shown in Figure 5A and Figure 5B. The biosensor showed wide linear range 5~150 μmol/L with a linear correlation

coefficient of 0.9915. The detection limit was 1.8 μmol/L. Copared with other work (Tabel S1), it still had its own advantage such as easy synthesis and low cost. To investigate the selectivity of the fabricated H_2O_2 biosensor, the anti-interference experiment was carried out (Figure 5C). It was observed that an obvious response after addition of 10 mM H_2O_2, while after addition of 100 mM glucose, ascorbic acid (AA), uric acid (UA), urea, NaCl and dopamine (DA) in the same sample, the current response kept relatively constant, suggesting that Cu_7S_4 nanocrystal had good selectivity for H_2O_2. Reproducibility tests were performed by measuring five different electrodes under the same condition. The relative standard deviation (RSD) of about 3.5 % was obtained. After storing at 4 ℃ for one month, the biosensor showed about 91.6 % of its initial response current. These results showed the biosensor had good reproducibility, selectivity and stability.

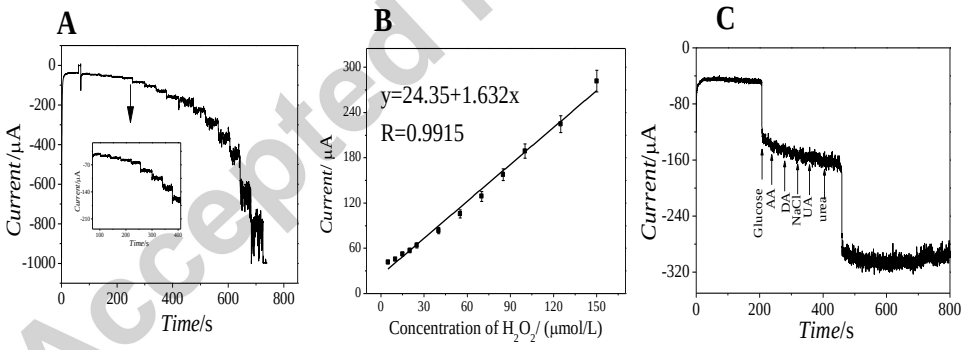

Figure 5 (A) Amperometric response of Cu_7S_4 nanocrystal/GCE with successive addition of H_2O_2 in 0.1 M PBS (inset: the current response of electrode toward the addition of H_2O_2); (B) Calibration curves of the Cu_7S_4 nanocrystal/GCE to different concentration of H_2O_2. Error bar = RSD (*n*=5); (C) Amperometric response of Cu_7S_4 nanocrystal/GCE toward the addition of H_2O_2 (10 mM) and various interfering compounds (10 mM respectively) in 0.1 M PBS solution.

3.5. Fabrication of a label-free immunosensor

Cu_7S_4 nanocrystal was also used to construct an electrochemical sensing platform for label-free detection of PSA as Figure 6 showed. CV was carried out in $K_4[Fe(CN)_6]$ solution to monitor the whole fabrication of the immunosenor as Figure 6A showed. When anti-PSA was immobilized on Cu_7S_4 nanocrystal/GCE via cross-linking with glutaraldehyde, the current declined sharply because anti-PSA hindered the electron transfer as protein. After the sequential introduction of BSA and PSA, current decreased continually. On one hand, BSA and PSA further hindered electron transfer. On the other hand, the immunoreation between PSA and anti-PSA would also cause the decrease of current. The result proved that the proposed immunosensor was successfully prepared.

I-t was further used to monitor the current response change during process towards 10 mM H_2O_2 as Figure 6B showed. After Cu_7S_4 nanocrystal was coated on GCE, the current response greatly increased towards H_2O_2 due to good electrocatalysis of Cu_7S_4 nanocrystal. After the sequential introduction of anti-PSA, BSA and PSA, current decreased continually because anti-PSA, BSA and PSA hindered electron transfer as biomolecules. The result further proved that the proposed immunosensor was successfully prepared.

3.6. Electrochemical characterization of the immunosensor

The prepared immunosensor was applied to detect PSA. As shown in Figure 6C, current response of the immunosensor decreased with increasing concentration of PSA. With concentration of PSA increasing, more PSA was captured by anti-PSA

resulting in gradually decreasing electrochemical signal response. A linear relationship between electrochemical response and concentration of PSA was obtained in the range of 0.001~15 ng/mL with the detection limit of 0.001 ng/mL (R=0.982) as Figure 6D showed. Although the sensitivity was not quite high compared with other work (Table S2), the sensitivity can still be acceptable which could be ascribed to the unique property and structure of Cu_7S_4 nanocrystal.

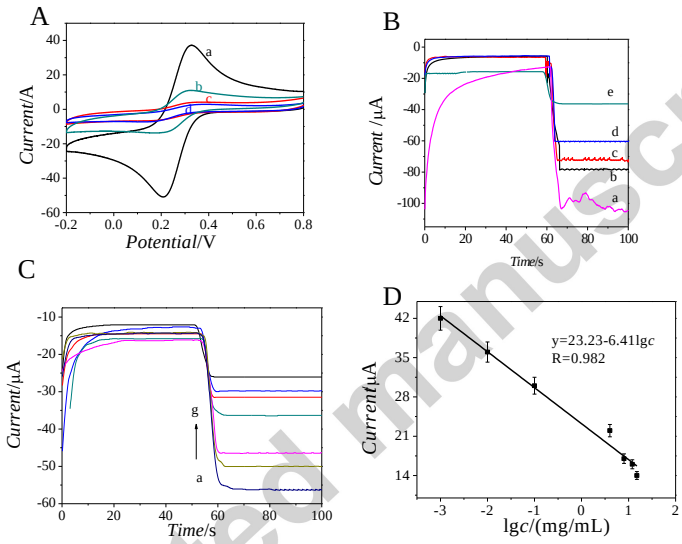

Figure 6 (A) CV of Cu_7S_4 nanocrystal/GCE (a), anti-PSA/Cu_7S_4 nanocrystal/GCE (b), BSA/anti-PSA/Cu_7S_4 nanocrystal/GCE (c) and PSA/BSA/anti-PSA/Cu_7S_4 nanocrystal/GCE (d) in 2 mmol/L $K_3[Fe(CN)_6]$ and 0.1 mol/L KCl solution; (B) Amperometric response of GCE (a), Cu_7S_4 nanocrystal/GCE (b), anti-PSA/Cu_7S_4 nanocrystal/GCE (c), BSA/anti-PSA/Cu_7S_4 nanocrystal/GCE (d) and PSA/BSA/anti-PSA/Cu_7S_4 nanocrystal/GCE (e) in 0.1 M PBS with 10 mM H_2O_2; (C) i-t of the immunosensor towards different concentrations of PSA: a 0.001 ng/mL, b 0.01 ng/mL, c 0.1 ng/mL, d 4 ng/mL, e 8 ng.mL, f 12 ng/mL, g 15 ng/mL. (D) Calibration curves of the Cu_7S_4 nanocrystal modified immunosensor to different concentration of PSA. Error bar =

RSD (n=5).

3.7. Reproducibility, selectivity and stability

Reproducibility, selectivity and stability were important factors to assess the performance of immunosensors. To assess the reproducibility of the proposed immunosensor, five different electrodes were prepared for the detection of 4 ng/mL of PSA and RSD of the measurements for five electrodes was 2.43 % as Figure S4A showed. The result demonstrated that the prepared immunosensor owned acceptable reproducibility.

To test the selectivity of the label-free electrochemical immunosensor, it was performed by adding the same concentration of alpha fetoprotein (AFP), Immunoglobulin G (IgG), and BSA into 4 ng/mL PSA. The variation of electrochemical signal response resulting from the interference was less than 5% compared with that without the interference as Figure S4B showed, suggesting the selectivity of the proposed immunosensor was acceptable.

The stability of the label-free electrochemical immunosensor was carried to monitor the electrochemical signal response periodicity. The fabricated immunosensor was stored at 4 ℃ when not in use. After storing for 3 weeks, the electrochemical signal response change for the detection of the same concentration of PSA was less than 7 % as Figure S4C showed. The proposed immunosensor showed acceptable reproducibility, selectivity and stability, therefore it was suitable for the quantitative detection of PSA in real human samples.

3.8. Real sample analysis

In order to assess the the practicability of the label-free electrochemical immunosensor, the detection of PSA in human serum samples was performed by using standard addition method. As shown in Table S3, the RSD was in the range from 1.0 % to 3.8 % and the recovery was in the range from 100.4 % to 113.0 %. The result implied that the immunosensor had great prospects in the quantitative detection of PSA in human serums.

4. Conclusions

In summary, Cu_7S_4 nanocrystal was prepared from Cu_2O precursor through simple solvothermal approach and Cu_7S_4 nanocrystal had the best electrochemical catalysis compared with CuS sphere and CuS flower. Due to the special structure of Cu_7S_4 nanocrystal, it possessed more exposed active point, higher surface area and lower Cu/S ratio. Therefore, Cu_7S_4 nanocrystal was used to construct a nonenzymatic biosensor for H_2O_2 and a label-free sensing platform for PSA. From the obtained experimental results, the biosensor possessed good sensitivity, selectivity and stability for H_2O_2 and PSA. This work demonstrated that Cu_7S_4 nanocrystal had potential application in electrochemical sensors due to its simple synthesis, low cost and good electrochemical performance.

5. Acknowledgements

This work was supported by the Shandong Provincial Natural Science Foundation of China (No. ZR2016BM01) and National Natural Science Foundation of China (Nos. 21575050 and 21375047).

Reference

Adhikari, S., Sarkar, D., Madras, G., 2017. ACS Omega 2, 4009-4021.

Cai, L.Y., Sun, Y.G., Li, W.Y., Zhang, W.L., Liu, X.J., Ding, D.R., Xu, N.N., 2015. RSC Adv. 5, 98136-98143.

Cao, H.L., Qian, X.F., Wang, C., Ma, X.D., Yin, J., Zhu, Z.K., 2005. J. Am. Chem. Soc. 127, 16024-16025.

Chen, Z.X., Zhang, W.X., Yang, Z.H., 2009. J. Cryst. Growth 311, 3347-3351.

Chen, Y.C., Shi, J.B., Wu, C., Chen, C.J., Lin, Y.T., Wu, P.F., 2008. Mater. Lett. 62, 1421-1423.

Chen, G.J., Ma, B., Wang, Y.Y., Xie, R.S., Li, C., Dou, K.F., Gong. S.Q., 2017. ACS Appl. Mater. Interfaces 9, 41700-41711.

Chen, W.L., Wang, M., Qian, T.Y., Cao, H.L., Huang, S.S., He, Q.Q., Liang, N., Wang, C., Zai, J.T., 2015. Nano Energy 12, 186-196.

Cui, J.B., Xu, S.Y., Wang, L.Y., 2017. Sci. China Mater. 60(4), 352-360.

Dutta, A.K., Das, S., Samanta, S., Samanta, P.K., Adhikary, B., Biswas, P., 2013. Talanta 107, 361-367.

Dutta, A.K., Das, S., Samanta, P.K., Roy, S., Adhikary, B., Biswas, P., 2014. Electrochim. Acta 144, 282-287.

Fan, G.C., Zhu, H., Du, D., Zhang, J.R., Zhu, J.J., Lin, Y.H, 2016. Anal. Chem. 88, 3392-3399.

Fu, T.X., 2013. Electrochim. Acta 112, 230-235.

Han, Y., Wang, Y.P., Gao, W.H., Wang, Y.J., Jiao, L.F., Yuan, H.T., Liu, S.X., 2011. Powder Technol. 212, 64-68.

Heydari, H., Moosavifard, E.S., Elyasi, S., Shahraki, M., 2017. App. Surf. Sci. 394, 425-430.

Hu, X.S., Shen, Y., Xu, L.H., Wang, L.M., Lu, L.S., Zhang, Y.T., 2016. App. Surf. Sci. 385, 162-170.

He, W.W., Jia, H.M., Li, X.X., Lei, Y., Li, J., Zhao, H.X., Mi, L.W., Zhang, L.Z., Zheng, Z., 2012. Nanoscale 4, 3501-3506.

Jia, X.L., Liu, Z.M., Liu, N., Ma, Z.F., 2014. Biosens. Bioelectron. 53, 160-166.

Jiang, Y.C., Zhang, S.D., Ji, Q., Zhang, J., Zhang, Z.P., Wang, Z.Y., 2014. J. Mater. Chem. A, 2, 4574-4579.

Kim, W.B., Lee, S.H., Cho, M., Lee, Y., 2017. Sens. Actuators, B 249, 161-167.

Li, Q., Wang, X.F., Tang, K., Wang, M.F., Wang, C., Yan, C.L., 2017. Acs nano 11, 12230-12239.

Lin, J.D., Tao, F.F., Wang, L.X., Chen, L.Z., Ying, Y.Q., Zhang, L.Q., Liu, H.L., Xia, M.Y., 2013. J Mater Sci 48, 5509-5516.

Liu, L.G., Zhong, H.Z., Bai, Z.L., Zhang, T., Fu, W.P., Shi, L.J., Xie, H.Y., Deng, L.G., Zou, B.S., 2013. Chem. Mater. 25, 4828-4834.

Ma, H.H., Sun, J.Z., Zhang, Y., Bian, C., Xia, S.H., Zhen, T., 2016. Biosens. Bioelectron. 80, 222-229.

Mousavi-Kamazani, M., Zarghami, Z., Salavati-Niasari, M., 2016. J. Phys. Chem. C 120, 2096-2108.

Oberpenning, F., Hetzel, S., Weining, C., Brandt, B., Angelis, A.G., Heinecke, A., Lein, M., Fornara, P., Schmid, H.P., Hertle, L., Semjonow, A., 2003. Eur. Urol. 43, 478-484.

Peng, W.C., Li, Y., Zhang, F.B., Zhang, G.L., Fan, X.B., 2017. Ind. Eng. Chem. Res. 56, 4611-4626.

Qian, L., Mao, J.F., Tian, X.Q., Yuan, H.Y., Xiao, D., 2013. Sens. Actuators, B 176, 952-959.

Raveau, B., Sarkar, T., 2011. Solid State Sci. 13, 1874-1878.

Rong, Y.M., He, K., Pacios, M., Robertson, W.A., Bhaskaran, H., Warner, H.J., 2015. ACS nano 9, 3695-3703.

Shi, F., Zheng, W.Z., Wang, W.C., Hou, F., Lei, B.X., Sun, Z.F., Sun, W., 2015. Biosens. Bioelectron. 64, 131-137.

Su, S., Han, X.Y., Lu, Z.W., Liu, W., Zhu, D., Chao, J., Fan, C., Wang, L.H., Song, S.P., Weng, L.X., Wang, L.H., 2017. ACS Appl. Mater. Interfaces 9, 12773-12781.

Tan, C.S., Hsu, S.C., Ke, W.H., Chen, L.J., Huang. H.M., 2015. Nano Lett., 15, 2155-2160.

Wang, N., Gao, C.Z., Han, Y., Huang. X.M., Xu, Y., Cao, X., 2015. J. Mater. Chem. B 3, 3254-3259.

Yang, Z.J., Cao, Y., Li, J., Lu, M.M., Jiang, Z.K., Hu, X.Y., 2016. ACS Appl. Mater. Interfaces 8, 12031-12038.

Yu, X.J., Bi, J.L., Yang, G., Tao, H.Z., Yang, S.C., 2016. J. Phys. Chem. C 120, 24533-24541.

Yu, X.L., Wang, Y., Chan, H.L.W., Cao, C.B., 2009. Micropor. Mesopor. Mat. 118,

423-426.

Zhang, S., Li, B.Q., Sheng, Q.L., Zheng, J.B., 2016. J. Electroanal. Chem. 769, 118-123.

Zhao, M., Chen, A.Y., Huang, D., Chai, Y.Q., Zhuo, Y., Yuan, R., 2017. Anal. Chem. 89, 8335-8342.

Highlights

•A label-free electrochemical immunosensor for PSA detection is constructed.

•18-facet polyhedron Cu_7S_4 nanocrystals was obtained through a simple solvothermal approach.

•A biosensor for H_2O_2 is constructed based on 18-facet polyhedron Cu_7S_4 nanocrystals.

• The immunosensor has been used to detect PSA in human serum sample.